Multi-Objective Aerodynamic Optimization of a High-Speed Train Head Shape Based on an Optimal Kriging Model

Y. Yang[1,5], Z. He[2,3,4], Z. Shi[1,5] and X. H. Xiong[2,3,4†]

[1] State Key Laboratory of Heavy Duty AC Drive Electric Locomotive Systems Integration
[2] Key Laboratory of Traffic Safety on Track, Ministry of Education, School of Traffic & Transportation Engineering, Central South University, Changsha, 410075, China
[3] Joint International Research Laboratory of Key Technology for Rail Traffic Safety, Central South University, Changsha, 410075, China
[4] National & Local Joint Engineering Research Center of Safety Technology for Rail Vehicle, Changsha, 410075, China
[5] CRRC Zhuzhou Locomotive Co.,Ltd. Zhuzhou 412001,China

†Corresponding Author Email: xhxiong@csu.edu.cn

ABSTRACT

An optimal Kriging surrogate model based on a 5-fold cross-validation method and improved artificial fish swarm optimization is developed for improving the aerodynamic optimization efficiency of a high-speed train running in the open air. The developed optimal Kriging model is compared with the original Kriging model in two test sample points, and the prediction errors are all reduced to within 5%. Thus, the optimal Kriging model is selected for use in each iteration to approximate the CFD simulation model of a high-speed train in subsequent optimization. After that, the strong Pareto evolutionary algorithm II (SPEA2) is adopted to obtain a series of Pareto-optimal solutions. Based on the above work, a multi-objective aerodynamic optimization design for the head shape of a high-speed train is performed using a free-form deformation (FFD) parameterization approach. After optimization, the aerodynamic drag coefficient of the head car and the aerodynamic lift coefficient of the tail car are reduced by 5.2% and 32.6%, respectively. The results demonstrate that the optimization framework developed in this paper can effectively improve optimization efficiency.

NOMENCLATURE

C_d	drag coefficient	β	weight coefficient
C_l	lift coefficient	δ	crowding factor
$D(i)$	density information of the individuals	θ_k	correlation parameter
H_1	nose height	X_i	current position of the *i-th* artificial fish
H_2	window height	Xc	central position of the fish swarm
L	nose length	y_i	true values of sample points
n_f	number of fish swarm in visual	$\hat{y}_i$	predicted values of sample points
P_0	origin point of the coordinate system	Y_i	objective function of artificial fish X_i
$P_{i,j,k}$	new positions of the control points	Y_j	random state in the range of vision
$S(i)$	number of individuals dominated by individual i		

1. INTRODUCTION

In recent years, with the rapid development of various computer simulation technologies such as finite element simulation, dynamic simulation, and fluid dynamics simulation, the reliability and accuracy of simulation experiments have also been greatly improved, and computer simulation technology has been widely used as a design aid. However, computer simulation technology still has some limitations. That is, the computational cost of computational simulation experiments is often too expensive and the cycle is too long (Yang *et al.* 2016). To solve the problem of high computational cost in computational simulation experiments (Venkataraman and Haftka 2004), the design method of using surrogate models to replace expensive computational simulation models came into being (Ong *et al.* 2005). The surrogate model is a mathematical modeling method that belongs to a branch of supervised machine learning. It can quickly and effectively realize the approximate fitting of multidimensional variables based on limited data information. It has been widely discussed and studied in many fields, such as optimization design, ecological modeling, geological statistics, artificial intelligence, and so on. Compared with the expensive computational simulation model, the surrogate model is a purely mathematical model, which can effectively reduce the calculation time and shorten the design cycle.

With the increasing speed of high-speed trains, aerodynamic drag and aerodynamic noise increase obviously, which affects the safety and stability of high-speed trains. The best way to reduce aerodynamic drag is to perform the aerodynamic optimization design of high-speed train head shapes (Tian 2019). Aerodynamic optimization design belongs to the category of multidisciplinary optimization design, which is widely used in the field of aerospace (Wang *et al.* 2014; Shen *et al.* 2020). In recent years, some scholars have applied the multidisciplinary optimization design method to the design of high-speed train heads to improve their aerodynamic performance. (Yao *et al.* 2014, 2016) used the NSGA-II algorithm to carry out aerodynamic optimization design for a simplified CRH380A model and improved the optimization efficiency by constructing a Kriging surrogate model. (Yu *et al.* 2019) proposed an efficient multi-objective aerodynamic optimization method based on a Kriging approximate model to improve the aerodynamic optimization efficiency of the high-speed train. (Zhang *et al.* 2016) proposed a multi-objective optimization design method for high-speed train head shape based on a Kriging surrogate model and a non-dominated sorting PSO algorithm combined with the proposed parameterization technique. (Li *et al.* 2016) optimized the aerodynamic performance of a high-speed train head shape by using a Kriging model and NSGA-II based on the FFD method, and obtained a set of Pareto-optimal solutions. (Sun *et al.* 2017) constructed a Kriging model that focused on the far-field noise level and the overall drag of a high-speed train, and the optimization design of the streamlined high-speed train head shape was performed. (Muñoz-Paniagua and García 2020) constructed a radial basis function (RBF) model for optimal candidates evaluation and accurate flow simulations using computational fluid dynamics (CFD), which largely speeds up the GA process. (Zhang *et al.* 2017a, b) proposed a multi-objective aerodynamic optimization method of the high-speed train head shape based on a kriging model and the NSGA-II algorithm, and obtained a series of Pareto-optimal solutions. After optimization, the aerodynamic drag of the whole train and the aerodynamic lift of the tail car were reduced by 2.61% and 9.9%, respectively.

The accuracy of surrogate models has an important impact on the results, and some scholars have made some efforts to improve the accuracy of surrogate models. (Xu *et al.* 2017) constructed a Kriging model by using a cross-validation method, and the optimization results showed that the Kriging model could effectively improve the optimization efficiency. (Zhang *et al.* 2019a) developed an optimal support vector regression model based on a radial basis kernel function for the small sample size and nonlinear characteristics of streamlined head optimization. (He *et al.* 2020) proposed a global optimization strategy based on the hybrid surrogate model and the CMOPSO algorithm to improve the accuracy of the aerodynamic performance optimization of a high-speed train head shape.

The surrogate models mentioned above mostly adopt original hyperparameters, and the prediction accuracy is difficult to guarantee. A surrogate model with original hyperparameters may cause poor prediction accuracy, which will directly affect the subsequent modeling process. Therefore, it is necessary to optimize the hyperparameters of the surrogate model. Moreover, an efficient optimization algorithm also has an important influence on optimization results. The artificial fish swarm algorithm (AFSA) is a new swarm intelligence algorithm that can solve some complex optimization problems. However, AFSA has a slow search speed, and it is easy to fall into a local optimum. In this paper, an optimal Kriging surrogate model is constructed based on a 5-fold cross-validation method and an improved AFSA. The minimizing mean square error (MSE) is considered as the optimization object, and an improved AFSA is then used to optimize the hyperparameters of the Kriging model to improve the prediction accuracy. Finally, a global optimization strategy based on the optimal Kriging surrogate model and the strong Pareto evolutionary algorithm 2 (SPEA2) is developed for the aerodynamic optimization design of a high-speed train head shape. After optimization, a set of Pareto optimal solutions are obtained, and the aerodynamic performance of the optimized high-speed train is compared with the original shape.

2. OPTIMAL KRIGING MODEL

2.1 Kriging model

The Kriging model is an unbiased estimation model with minimum estimation variance, which has the characteristics of local estimation. It was first proposed by Danie Krige, a geologist in South Africa, in 1951. Kriging is an optimized interpolation algorithm, which simulates interpolation through a Gaussian process controlled by covariance to generate continuous functions. This method not only considers the influence of the distance relationship between sample points on output variation but also considers the influence of the location relationship and spatial distribution of sample points on the overall output (Li 2017). The expression consists of two parts, as in Eq. (1).

$$y(\mathbf{x}) = \sum_{i=1}^{k} \beta_i f_i(\mathbf{x}) + z(\mathbf{x}) \tag{1}$$

where $y(\mathbf{x})$ denotes known approximate function, β_i denotes unknown weight coefficient, and $z(\mathbf{x})$ represents random process, which is usually a standard Gaussian random distribution equation with a mean value of 0 . The variance is

$$con[z(\mathbf{x}_i), z(\mathbf{x}_j)] = \sigma^2 \, \mathrm{R}[R(\mathbf{x}_i, \mathbf{x}_j)] \tag{2}$$

where σ^2 is the process variance, R is the matrix of covariance, and $R(\mathbf{x}_i, \mathbf{x}_j)$ is the relationship function of the input variables $\mathbf{x}_i$ and $\mathbf{x}_j$. In this paper, a Gaussian correlation function was used, and its expression can be expressed by the following equation.

$$R(\theta, x^i, x^j) = \exp[-\sum_{k=1}^{m} \theta_k \left| x_k^i - x_k^j \right|^2], \ (i, j = 1, \dots, n) \tag{3}$$

where m represents the number of design variables, θ_k is the unknown correlation parameter. x_k^i and x_k^j represent the *k-th* components of sample points x^i and x^j, respectively.

θ_k has an important influence on the prediction accuracy of Kriging model. The essence of constructing Kriging model is to determine the optimal θ_k value. If θ_k was considered as the independent variable, and the mean square error (MSE) was considered as the optimization objective. The optimal θ_k of the correlation function can be obtained by solving the following equation.

$$\begin{cases} Minimise \quad \varphi(\theta_k) = \frac{n}{2}\ln(\hat{\sigma}^2) + \frac{1}{2}\ln(|R|) \\ Subject \ to: \ \theta_k > 0 \end{cases} \tag{4}$$

In the above equation, both $\hat{\sigma}^2$ and $|R|$ are functions of θ_k. The artificial fish swarm optimization algorithm (AFSA) will be used to find

the optimal θ_k. The relevant theory will be introduced in the next section.

2.2 Artificial fish swarm optimization

The artificial fish swarm algorithm (AFSA) is a new swarm intelligence algorithm that can solve some complex model optimization problems. The algorithm has the advantages of strong adaptive ability, fast convergence speed, and strong robustness, and has become an important swarm intelligence algorithm (Liu and Yuan 2020). AFSA can search for global optimization through simulating the foraging, tailing, clustering, and random behaviors of the fish swarm. The behaviors are as follows:

2.2.1 Foraging behavior

Foraging behavior indicates the aggregation behavior of artificial fish in places with a high food concentration. The fish in location x_i performs updating the next new state x_j within the visual range, and its behavior formula is as follows.

$$x_j = x_i + visual \cdot rand \tag{5}$$

$$X_i^{k+1} = X_i^k + rand \cdot step \cdot \frac{X_j - X_i^k}{\left\| X_j - X_i^k \right\|} \tag{6}$$

where X_i is the current position of the *i-th* artificial fish, and X_j represents the random state in the range of vision. *rand* represents the random number between 0 and 1. *step* represents the moving step size, and k denotes the time. If in the maximum problem, namely $Y_i < Y_j$, the artificial fish will move one step toward this direction, otherwise the random behavior will be executed.

2.2.2 Clustering behavior

If the fish swarm is dense, it means that the probability of the optimal solutions is the largest, but at the same time, excessive aggregation should be avoided. The central position of the fish swarm is defined as X_c, and the objective function of artificial fish X_i is Y_i. The number of fish swarm in vision is n_f, and the central position of visual field can be expressed as $X_c = \sum_{j=1}^{n_f} x_j / n_f$. if $Y_c > Y_i$ and $n_f / N < \delta$, which means that there are many excellent individuals in the center of visual range, and artificial fish can move toward the central position because there are not overcrowding. Otherwise, the foraging behavior will perform (Luo *et al.* 2020). The formula can be expressed as

$$X_i(t+1) = X_i(t) + rand \cdot step \cdot \frac{X_c(t) - X_i(t)}{\left\| X_c(t) - X_i(t) \right\|}, \ Y_c > Y_j \tag{7}$$

2.2.3 Tailing behavior

$$X_i^{k+1} = X_i^k + rand \cdot step \cdot \frac{X_{max} - X_i^k}{\|X_{max} - X_i^k\|} \qquad (8)$$

where X_i^k is the current position of artificial fish. If $Y_{max}/n_f > \delta Y_i$, it will move one step to X_{max}. Otherwise, the foraging behavior will be executed.

2.2.4 Random behavior

$$X_i^{k+1} = X_i^k + rand \cdot visual \qquad (9)$$

Random behavior is the default behavior of foraging behavior. In foraging behavior, artificial fish will randomly select a position and move to this position after a certain number of exploratory times.

2.3 Improved artificial fish swarm algorithm

In the AFSA algorithm, if the visual range is set to be larger, the fish detection range will be wider, which is beneficial to tailing and clustering behavior. On the contrary, if the range is smaller, the search will be more detailed, which is beneficial to the convergence speed, but it is easy to fall into the local optimum (Zhang *et al.* 2019; Chen 2019; Yu and Jin 2018). Therefore, a polynomial function is proposed to adaptively adjust the visual field. The fish swarm searches over a large range in the early stages and a small range in the latter stages, which can improve the search accuracy and convergence speed. The formula is in Eq. (10).

$$\begin{cases} visual = visual_{min} + \mu(visual_{max} - visual_{min}) \\ \mu = 1 - t/T_{max} \end{cases}$$

$$(10)$$

where $visual_{min}$ and $visual_{max}$ represent the minimum and maximum values of the visual range. t represents the current number of iteration, and T_{max} represents the maximum number of iteration.

The crowding factor δ represents the number of artificial fish that can be accommodated in a unit volume, and the range is between 0 and 1. This value in most of the literature is set to 0.618. In order to prevent the AFSA algorithm from falling into a local optimum, a smaller δ in the early stages can enhance the global search ability of the AFSA, and a larger δ in the latter stages can make the fish swarm gather in an optimal area, which considers the search ability and convergence speed of the algorithm simultaneously. The improved crowding factor is in Eq. (11).

$$\delta = \delta_{min} + \delta_{min} e^{1 - T_{max}/t} \qquad (11)$$

where δ_{min} is the minimum crowding factor, which is set to 0.382 here. t represents the current iteration, and T_{max} represents the maximum iteration number.

2.4 Evaluation method of surrogate model

When using the surrogate model to predict unknown data points, only reasonable parameter values and training methods can obtain ideal prediction accuracy. To avoid overfitting and underfitting in the process of constructing a surrogate model, on the one hand, the k-fold cross-validation (CV) method was used to train the sample points. That is, divide the sample points into k groups and select one group as the test set, while the remaining k-1 groups are selected as the training set. After iterations, a total of k models and k prediction errors are obtained. The final evaluation index is calculated by averaging the k errors, where k = 5. On the other hand, the optimization algorithm is used to optimize the parameters. In the optimization process, the error obtained each time is evaluated by the mean square error (MSE), and the expression is presented in Eq. (12).

$$MSE = \frac{1}{n} \sum_{i=1}^{n} (y_i - \hat{y}_i)^2 \qquad (12)$$

where n denotes the number of sample points. y_i and $\hat{y}_i$ represent the true value and predicted value, respectively. *MSE* is a commonly used method that can evaluate the error between the predicted value and the true value on the entire design interval. For a model with higher prediction accuracy, the *MSE* should be as small as possible. The value of the *MSE* should be positive, and its magnitude is affected by the output magnitude of the original problem.

3. AERODYNAMIC OPTIMIZATION DESIGN

3.1 The total optimization framework

The aerodynamic optimization framework proposed in this paper uses a global optimization method based on an optimal Kriging model and the strong Pareto evolutionary algorithm 2 (SPEA2), as shown in Fig. 1. The steps are as follows:

(1) The optimal Latin hypercube sampling (Opt. LHS) is used, and the results are saved in the sample database.

(2) After the mesh is deformed by the FFD method, a high-precision computational fluid dynamics (CFD) simulation is carried out to obtain the corresponding response values for each sample, which are stored in a sample database. Then the data are normalized.

(3) The Kriging model with an initial parameter is constructed based on k-fold cross validation, and MSE is used to evaluate the error.

(4) If the error satisfies the requirement, then the optimal Kriging model is obtained. Otherwise, the improved artificial fish swarm algorithm is used to search for the optimal parameter, and the algorithm then returns to step (3).
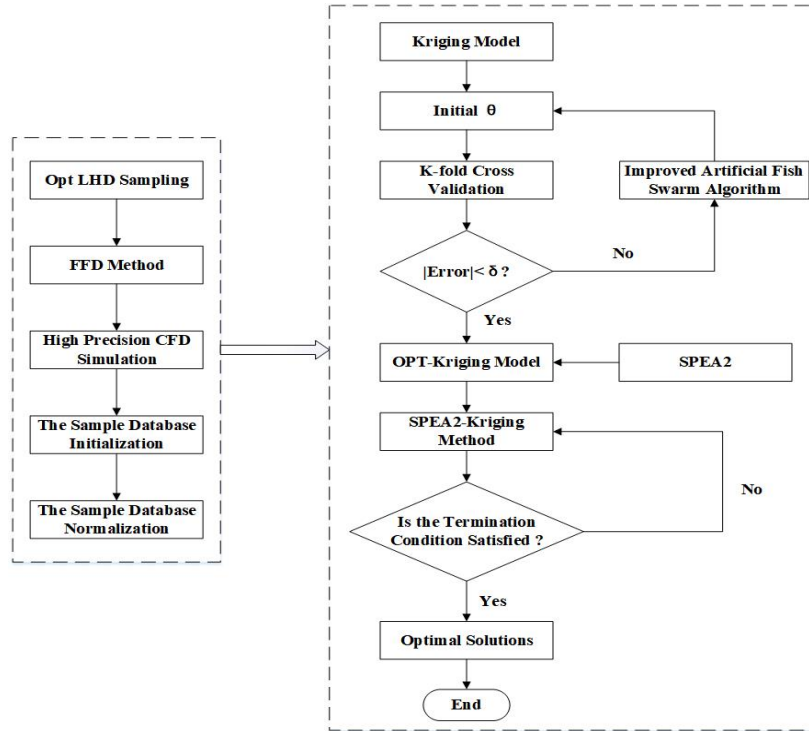
Fig. 1. Flowchart of a global optimization method based on the optimal Kriging model and the strong Pareto evolutionary algorithm 2.

(5) The strong Pareto evolutionary algorithm 2 (SPEA2) is used to obtain the initial optimal solution set. If the initial optimal solution set satisfies the requirement, then the final Pareto front is obtained. Otherwise, the new sample points are added to the sample database, and the algorithm then returns to step (4).

3.2 FFD method

This FFD method was first proposed by Sederberg and Parry in 1986 (Thomas and Parry 1986), and can be expressed in terms of mathematical relations as follows: By moving the control points, the grid nodes are moved along with the control points in accordance with a certain functional relationship, and the new global coordinates of the control points are obtained. Thus, the deformation of the grid is realized. In a Cartesian coordinate system, the target entity is constrained in an $l \times m \times n$ parallel hexahedral lattice, and a control vertex $P(x, y, z)$ satisfies the following formula (He *et al.* 2020).

$$P_{i,j,k} = P_0 + \frac{i}{l} \cdot X + \frac{j}{m} \cdot Y + \frac{k}{n} \cdot Z \qquad (13)$$

where P_0 is the origin point of the coordinate system; i=0, 1, 2,…,l; j=0,1,2,…,m and k=0,1,2,…,n. For any point Q, when the mesh is deformed by moving the control points, the deformation function is defined by a trivariate tensor product of Bernstein polynomials. The new coordinate position of Q is

$$Q_{ffd} = \sum_{i=0}^{l} \sum_{j=0}^{m} \sum_{k=0}^{n} B_{i,l}(x) B_{j,m}(y) B_{k,n}(z) P_{i,j,k} \qquad (14)$$

where $P_{i,j,k}$ are the new coordinate positions of the control points after deformation. $B_{i,l}(x)$, $B_{j,m}(y)$ and $B_{k,n}(z)$ are the Bernstein basis functions, which are expressed as follows:

$$B_{i,l}(x) = \frac{l!}{i!(l-i)!} x^i (1-x)^{l-i} \qquad (15)$$

$$B_{j,m}(y) = \frac{m!}{j!(m-j)!} y^j (1-y)^{m-j} \qquad (16)$$

$$B_{k,n}(z) = \frac{n!}{k!(n-k)!} z^k (1-z)^{n-k} \qquad (17)$$

The mesh deformation can maintain C1 continuity. In this paper, the deformation region mainly lies in the nose height, window height, and the nose length, which are expressed as $H1$, $H2$, and L, respectively. The deformation of the mesh was controlled by a series of control points. The ranges of the design variables and the corresponding coordinates of control points are shown in Table 1. An arbitrary shape deformation (ASD) control body was established, as shown in Fig. 2. The control points of each part are marked in yellow, and mesh deformation was realized by moving the control points.

3.3 CFD simulation

The study aims to optimize a simplified 1:1 model of high-speed train head with a three-car configuration. The influence of the bogies and the windshield on the aerodynamic force of the high-speed train are considered. The total length of the

Table 1 Ranges of the three design variables and the corresponding coordinates of control points

Design variable (mm)	Initial value	Lower bound	Upper bound	coordinates of control point
H_1	0	-150	100	(-38278.7,10000,1947.86)、(38282.2,10000,1947.86)
H_2	0	-100	100	(-35085.1,10740.6,5193.64)、(-35085.1,9259.38,5193.64)、(-34286.7,10740.6,5193.64)、(-34286.7,9259.38,5193.64)、(35088.7,9259.38,5193.64)、(35088.7,10740.6,5193.64)、(34290.3,9259.38,5193.64)、(34290.3,10740.6,5193.64)
L	0	-50	150	(-38278.7,10740.6,1947.86)、(-38278.7,9259.38,1947.86)、(38282,10740.6,1947.86)、(38282,9259.38,1947.86)
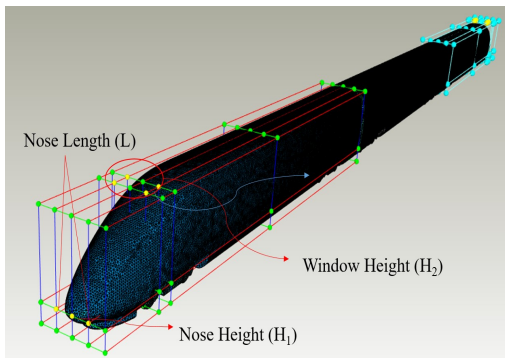
Fig. 2. ASD volume for the high-speed train and the deformation of the three parts of the train head.
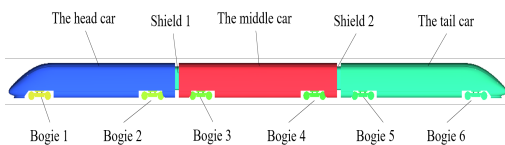

Fig. 3. Train model.

train is about 76.5 m, in which the lengths of the head car and the tail car are each 25.68 m, and the length of the middle car is 24.78 m. The height of the high-speed train is 3.89 m, and the width is 2.95 m. The geometric model is shown in Fig. 3.

In this paper, the octree algorithm in the ICEM CFD software was used to discretize the domain. The space was divided into tetrahedral grid cells. The surfaces of the train were divided into triangular grid cells, and fine prism grid cells were used around the train body. Take the total length of the train, L, as the characteristic length, and the computational domain extends L ahead of the train nose and 2L from the train tail to the exit of the computational domain. The top of the computational domain is at a distance of 0.5L from

the bottom of the rail, and the sides are at a distance of 0.5L from the center axis of the train. The outline of the computational domain and the model are shown in Fig. 4.

The running speed of this train in the open air without a crosswind is 300 km/h. The Mach number is 0.245, which is less than 0.3, thus, the air compressibility is not considered. Therefore, the three-dimensional steady incompressible Navier-Stokes (N-S) equation was used to simulate the flow field around the train based on the finite volume method. The Reynolds averaged N-S equations (RANS) method was used to solve this equation (Blazek 2005). The reference area is 11.2 m². The k-w SST model was selected as the turbulence model. The standard wall boundary functions were used near the walls to ensure the accuracy of the CFD results with a limited amount of mesh. The entrance of the domain was set to the velocity-inlet boundary conditions and the exit of the domain was set to the pressure-outlet boundary conditions. The two sides and the top of the computational domain were all set to symmetrical boundary conditions, and the train body is a nonslip solid wall boundary condition. The ground is treated as a moving wall to simulate the ground effect, and the moving speed is equal to the train speed. The CFD simulation was performed in starCCM software. The residual of continuity is set to 0.0001, which is considered as the convergence criterion.

4. RESULTS AND DISCUSSION

4.1 Sample points and prediction accuracy

The design of experiment (DOE) is to generate some sample points in the design space to approximately represent the whole design space and to reduce the computational complexity of the optimization algorithm by constructing an approximate model. Common DOE methods
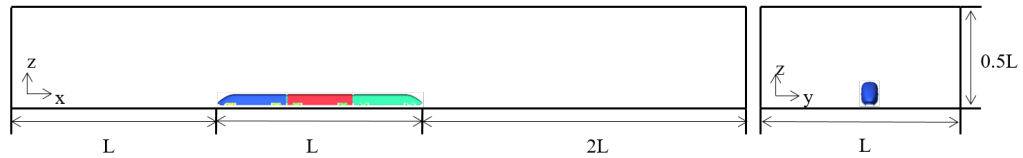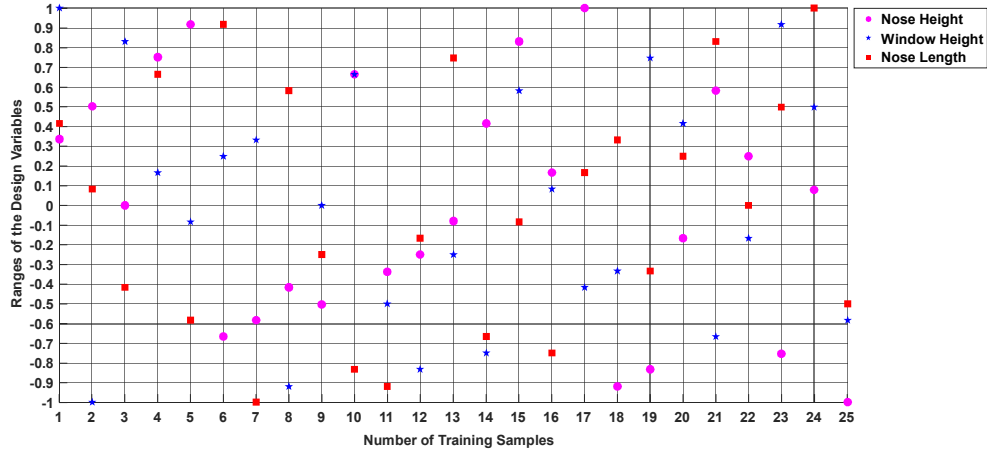
Fig. 4. Computational domain.

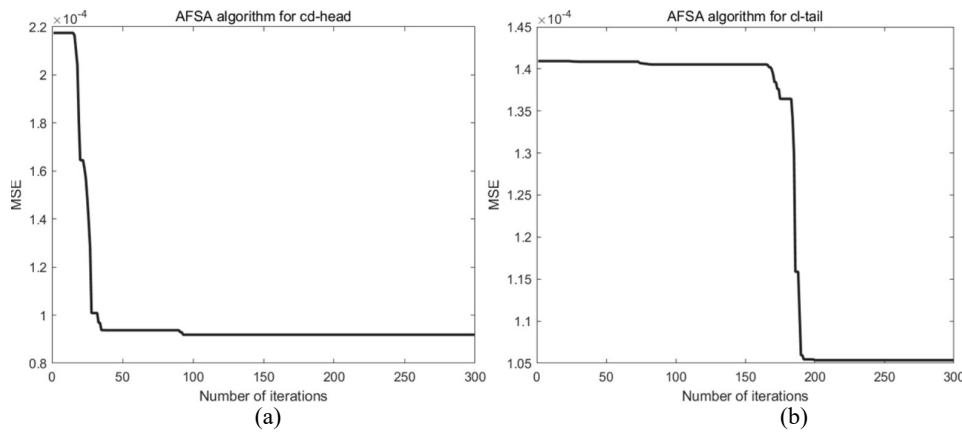**Fig. 5. Plane distributions of the training samples.**

Fig. 6. Hyperparameter optimization curves conducted by AFSA. (a) Kriging model constructed by drag coefficient of the head car (b) Kriging model constructed by lift coefficient of the tail car.

include full factor design, orthogonal experimental design, and optimal Latin hypercube experimental design (Opt. LHS). The head shape of a high-speed train is a complex streamlined shape. In this paper, three main design variables were selected to generate 25 training sample points in the design space using an Opt. LHS, and two random sample points (-100, 0, 100; 100, 50, -50) were generated in the design space for prediction accuracy testing (He *et al.* 2020). The plane distributions of the training samples are plotted in Fig. 5.

This paper constructed the Kriging surrogate model based on a k-fold cross-validation method, where k is set to 5. That is, we divided the sample points into k groups and selected one group as the test set, and the remaining k-1 groups were selected as the training set. After iterations, a total of k models and k mean square errors (MSE) are obtained, and the average of these k mean square errors is used as the final error output. The Gaussian function was selected as the correlation function. The improved

artificial fish swarm algorithm is used to optimize the hyperparameters of the Kriging model. In the optimization process, the hyperparameters of the Kriging model were used as the input variables, and their dimension is the same as the design variable dimension of the high-speed train in this paper. The mean square error (MSE) is considered as the output variable. The number of artificial fish is set to 50, and the search range is (0.001, 20). The minimum and maximum vision are set to 0.5 and 5, respectively. The maximum number of attempts is set to 20, the step is set to 0.5, and the maximum number of iterations is set to 300. The hyperparameter optimization curves of the Kriging model for drag coefficient and lift coefficient is shown in Fig. 6. The optimal Kriging model is compared with the original Kriging model. The initial hyperparameters are all set to 0.1, while after optimization, the hyperparameters are changed to 0.0026, 20, and 0.2032 for the aerodynamic drag coefficient, and 0.1626, 10.2485, and 0.2773 for the lift coefficient of the tail car, respectively. The

Table 2 Prediction error comparison

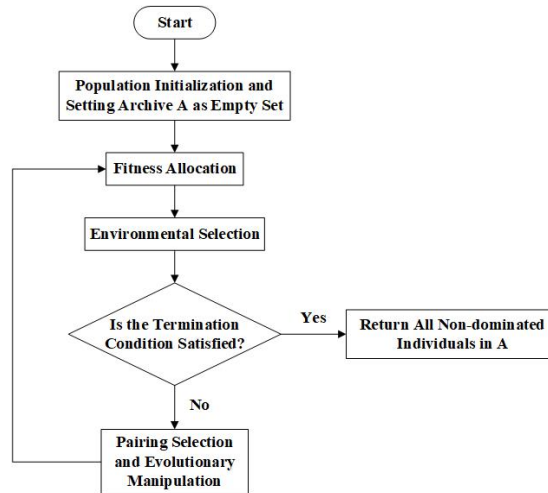| Objective	Points	Actual value	Original Kriging model	Error	Optimal Kriging model	Error
C_d-head	Test1	0.1513	0.1458	3.6%	0.1541	1.9%
	Test2	0.1693	0.1470	13.2%	0.1625	4%
C_l-tail	Test1	0.0906	0.0980	8.2%	0.0878	3.1%
	Test2	0.0735	0.1244	69.3%	0.0702	4.5%

Fig. 7. Flowchart of SPEA2.

prediction error of the original Kriging model for the aerodynamic drag coefficient is about 3%~14%, while the error of the optimal Kriging model is reduced to within 5%. For the aerodynamic lift of the tail car, the original Kriging performed poorly, and the prediction errors were reduced to within 5% after optimization. It can be observed that the aerodynamic lift coefficient of the tail car is more sensitive to the input parameters of the Kriging model. The details are shown in Table 2. Hence, the optimal Kriging models can meet the accuracy requirement.

4.2 Multi-objective optimization

4.2.1 Introduction of SPEA2

SPEA2 (Zitzler *et al.* 2002) is an adaptation of the original strong Pareto evolutionary algorithm (SPEA) proposed by (Zitzler and Thiele 1999). Compared with the SPEA algorithm, the SPEA2 algorithm has made improvements in the individual evaluation and the environmental selection mechanism. To avoid that evolutionary population individuals dominated by the same external population individuals have the same fitness value, the SPEA2 algorithm considers the dominance and dominated information of the individual when calculating the fitness value of the individual. The fitness function (Zhu *et al.* 2019) is defined as follows.

$$\begin{cases} f(i) = R(i) + D(i) \\ R(i) = \sum_{j \in P_t + P_t^*, i < j} S(j) \\ S(i) = \left| \left\{ j \mid j \in P_t \cup P_t^* \wedge j \prec i \right\} \right| \\ D(i) = \dfrac{1}{2 + \sigma_i^k} \end{cases} \qquad (18)$$

where $S(i)$ represents the number of individuals dominated by individual i. $R(i)$ represents the sum of the number of other individuals dominated by all individuals j dominating i in the evolutionary population P_t and the external population P_t^*. $D(i)$ is the density information of the individuals, and σ_i^k represents the Euclidean distance from individual i to k-th individual, where $k = \sqrt{N + M}$, N denotes the capacity of the evolutionary population, and M is the capacity of the external population. By defining the fitness function in the above formula, we can get not only the dominance and non-dominated information of individuals, but also the distribution of individuals in the population. In addition, in the environmental selection mechanism, the capacity of the external population set by the SPEA2 algorithm is unchanged. When the selected non-dominated individuals exceed the capacity of the external population, they need to be cut. The SPEA2 algorithm can obtain a better distributed external population through this cut strategy. The whole process is shown in Fig. 7.

4.2.2 Analysis of optimization results

In this paper, SPEA2 was used for multi-objective aerodynamic optimization of a high-speed train head shape, and an optimal Kriging model obtained in the previous section was used as the surrogate model. The population size is set to 50, and the maximum number of iterations is 500. Finally, the Pareto front for the aerodynamic drag coefficient and the lift coefficient is obtained, as shown in Fig. 8. It can be seen from the figure that there is a non-
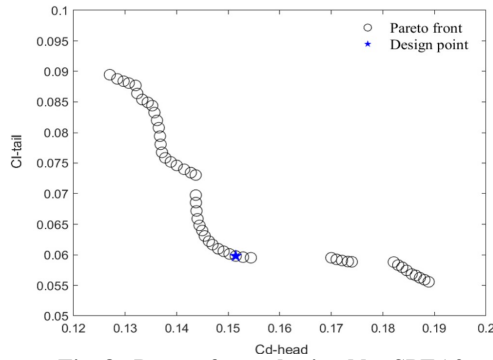
Fig. 8. Pareto front obtained by SPEA2.

dominant relationship between the aerodynamic drag coefficient of the head car and the lift coefficient of the tail car. A suitable solution marked with an asterisk in the figure is selected as the final optimal design point under consideration. The original aerodynamic force coefficients obtained by CFD simulation were verified by (Liang *et al.* 2020), and the errors are 0.4% and 4.5%, respectively. Besides, the results are also compared with the wind tunnel tests, and the maximum error is less than 10% for aerodynamic drag coefficient, and no more than 5% for aerodynamic lift coefficient (Li *et al.* 2019; Xia *et al.* 2017c). After optimization, The drag coefficient of the head car and lift coefficient of the tail car are 0.1514 and 0.06. The errors are 0.79% and 20%,

respectively. Compared with the original head shape, it reduced by 5.2% and 32.6%, respectively, as shown in Table 3. The optimal values of the design variables are 34.258 mm (H_1), -25.756 mm (H_2), 145.633 mm (L), where positive values mean that a certain part of the high-speed train becomes

longer or higher, and negative values mean shorter or lower. The change of each design variable will produce a certain degree of deformation on the specific position of the shape, and the final shape after optimization is coupled by all design variables, which is the result of the comprehensive action of all variables.

Table 3 Aerodynamic forces reduction after SPEA2 optimization

Model	C_d-head	C_l-tail
Original	0.1597	0.089
Liang *et al.* 2020	0.1590	0.093
Error (%)	0.4	4.5
Optimal	0.1514	0.060
CFD simulation	0.1526	0.072
Error (%)	0.79	20
Reduction (%)	5.2	32.6

The head shapes of the high-speed train before and after optimization is shown in Fig. 9. We can see from the deformation figure that the optimal head shape is coupled by all design variables, and the deformation mainly occurred in the nose length. To better understand the influence of the changing head shape on the aerodynamic performance of high-speed trains before and after optimization, the flow field of the high-speed train before and after optimization was analyzed. The pressure distribution diagram of the head car is shown in Fig. 10. It can be seen from the figure that the red color at the nose cone is obviously weakened, which proves that the optimized high-speed train reduces the pressure to a certain extent, and it also shows the effectiveness of the multi-objective optimization framework developed in this paper.
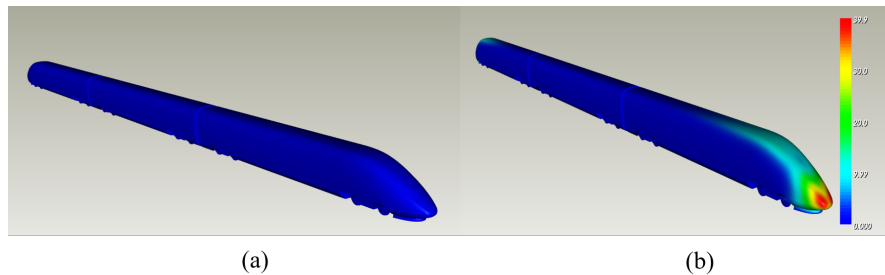

(a)   (b)

Fig. 9. Comparison of the original high-speed train head shape with an optimal head shape. (a) The original train and (b) the optimal train.
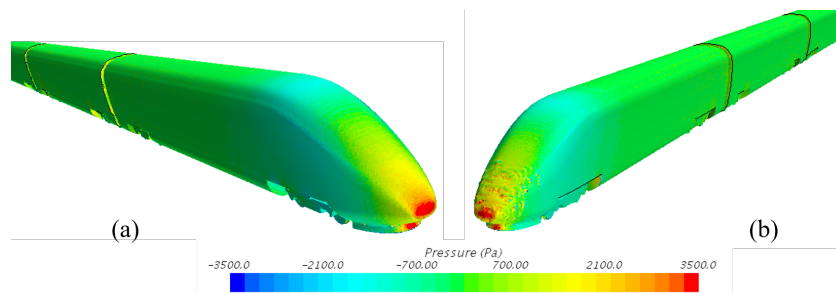

(a)   (b)

Fig. 10. Comparison of the pressure distributions of the original train and an optimal train: (a) the original train and (b) the optimal train.

5. CONCLUSION

In the present paper, with limited sample points, a hyperparameter optimization strategy based on a Kriging surrogate model and artificial fish swarm algorithm (AFSA) was developed. An improved AFSA using an adaptive method was proposed to improve the optimization efficiency. The test results of two sample points proved that the optimal Kriging model can meet the accuracy requirement.

After that, a global aerodynamic optimization framework for a high-speed train head shape was built based on the optimal Kriging surrogate model. The FFD method was adapted for deforming the mesh, which avoided the remodeling of the grids and geometric models, greatly reducing the modeling time and improving the parameterization efficiency. A high-precision CFD simulation model was employed to obtain good aerodynamic performance. A strong Pareto evolutionary algorithm 2 (SPEA2) was used to obtain a set of Pareto-optimal solutions. The results showed that the Pareto front obtained by the drag coefficient and lift coefficient was well distributed. The drag coefficient of the head car is reduced by 5.2%, and the lift coefficient of the tail car is reduced by 32.6% after optimization, which proves the effectiveness of the global optimization framework developed in this paper.

ACKNOWLEDGEMENTS

REFERENCES

Blazek, J. (2005). Computational fluid dynamics: principles and applications. *Elsevier*, Butterworth-Heinemann, Oxford.

Chen, J. Z. (2019). Robot path planning and tracking based on improved artificial fishswarm algorithm. *Mechanical Design and Manufacturing* 4, 251-255.

He, Z., X. H. Xiong, B. Yang and H. H. Li (2020). Aerodynamic optimisation of a high-speed train head shape using an advanced hybrid surrogate-based nonlinear model representation method. *Optimization and Engineering* 1-26.

Li, J. L. (2017). *Development and Application of Extended Adaptive Hybrid Surrogate Model.* Dalian University of Technology.

Li, R., P. Xu, Y. Peng and P. Ji (2016). Multi-objective optimization of a high-speed train head based on the FFD method. *Journal of Wind Engineering and Industrial Aerodynamics* 152, 41-49.

Li, X. B., G. Chen, Z. Wang, X. H. Xiong, X. F. Liang and J. Yin (2019). Dynamic analysis of the flow fields around single- and double-unit trains. *Journal of Wind Engineering and Industrial Aerodynamics* 188, 136-150.

Liang, X. F., X. Zhang, G. Chen and X. B. Li (2020). Effect of the ballast height on the slipstream and wake flow of high-speed train. *Journal of Wind Engineering and Industrial Aerodynamics* 207, 104404.

Liu, G. B. and H. J. Yuan (2020). Improved Artificial Fish Swarm Algorithm to Optimize SVR Prediction Model. *Journal of Huaiyin Teachers College (Natural Science Edition)* 19(3), 207-211.

Luo, R. X., M. Chen and J. Lin (2020). Robot path planning based on improved artificial fish swarm algorithm. *Science Technology and Engineering* 20(23), 9445-9449.

Muñoz-Paniagua, J. and J. García (2020). Aerodynamic drag optimization of a high-speed train. *Journal of Wind Engineering and Industrial Aerodynamics* 204, 104215.

Ong, Y. S., P. B. Nair, A. J. Keane and K. W. Wong (2005). Surrogate-assisted evolutionary optimization frameworks for high-fidelity engineering design problems. In *Knowledge Incorporation in Evolutionary Computation*, Heidelberg, Berlin.

Sederberg, T. W., and S. R. Parry (1986). Free-form deformation of solid geometric models. In *Proceedings of the 13th annual conference on Computer graphics and interactive techniques* 20(4), 151-160.

Shen, Y., W. Huang, L. Yan and T. T. Zhang (2020). Constraint-based parameterization using FFD and multi-objective design optimization of a hypersonic vehicle. *Aerospace Science and Technology* 100, 105788.

Sun, Z. X., Y. Zhang and G. W. Yang (2017). Surrogate based optimization of aerodynamic noise for streamlined shape of high speed trains. *Applied Sciences* 7(2), 196.

Tian, H. Q. (2019). Review of research on high-speed railway aerodynamics in China. *Transportation Safety and Environment* 1(1), 1-21.

Venkataraman, S. and R. T. Haftka (2004). Structural optimization complexity: what has Moore's law done for us. *Structural and Multidisciplinary Optimization* 28(6), 375-387.

Wang, Z. G., W. Huang and L. Yan (2014). Multidisciplinary design optimization approach and its application to aerospace engineering. *Chinese Science Bulletin* 59(36), 5338–5353.

Xia, C., H. F. Wang, X. Z. Shan, Z. G. Yang and Q. L. Li (2017c). Effects of ground configurations

on the slipstream and near wake of a high-speed train. *Journal of Wind Engineering and Industrial Aerodynamics*. 168, 177-189.

Xu, G., X. F. Liang, S. B. Yao, D. W. Chen and Z. W. Li (2017). Multi-objective aerodynamic optimization of the streamlined shape of high-speed trains based on the Kriging model. *Plos One* 12(1), e0170803.

Yang, J. Q., Z. F. Zhan, K. Zheng, J. Hu and L. Zheng (2016). Enhanced similarity-based metamodel updating strategy for reliability-based design optimization. *Engineering Optimization* 48(12), 2026-2045.

Yao, S. B., D. L. Guo, Z. X. Sun, D. W. Chen and G. W. Yang (2016). Parametric design and optimization of high speed train nose. *Optimization and Engineering* 3(17), 605-630.

Yao, S. B., D. L. Guo, Z. X. Sun, G. W. Yang and D. W. Chen (2014). Optimization design for aerodynamic elements of high speed trains. *Computers & Fluids* 95, 56-73.

Yu, M. G., J. K. Pan, R. C. Jiang and J. Y. Zhang (2019). Multi-objective optimization design of the high-speed train head based on the approximate model. *Journal of Mechanical Engineering* 55(24), 178-186.

Yu, Z. X. and Y. J. Jin (2018). Parameter estimation of regression model based on improved artificial fish swarm algorithm. *Statistics and Decision* 34(22), 75-77.

Zhang, L., J. Y. Zhang, T. Li and Y. D. Zhang (2017a). Multi-objective optimization design of the streamlined head shape of super high-speed trains. *Journal of Mechanical Engineering* 53(2), 106–114.

Zhang, L., J. Y. Zhang, T. Li and Y. D. Zhang (2017b). A multiobjective aerodynamic optimization design of a high-speed train head under crosswinds. *Journal of Rail and Rapid Transit* 232(3), 895–912.

Zhang, M. X., P. Wang and Y. P. Bai and Y. C. Hou (2019). DOA estimation of array signal based on IAFSA-MUSIC algorithm. *Mathematical Practice and Understanding* 49(22), 163-170.

Zhang, Y., G. W. Yang, D. L. Guo, Z. X. Sun and D. W. Chen (2019a). A novel CACOR-SVR multi-objective optimization approach and its application in aerodynamic shape optimization of high-speed train. *Soft Computing* 23(13), 5035-5051.

Zhang, Y., G. W. Yang, Z. X. Sun and D. L. Guo (2016). A general shape optimization method based on FFD approach with application to a high-speed train. *Journal of Multidisciplinary Engineering Science and Technology* 3(12), 6181-6188.

Zhu, W. Q., W. L. Yang, S. Ku and J. Wang (2019). Multi-objective Maneuvering Trajectory Planning Based on SPEA2 Algorithm for UCAV. *Unmanned Systems Technology* 2(6), 23-33.

Zitzler, E. and L. Thiele (1999). Multiobjective evolutionary algorithms: a comparative case study and the strength Pareto approach. *IEEE transactions on Evolutionary Computation* 3(4), 257-271.

Zitzler, E., M. Laumanns and L. Thiele (2002). Improving the Strength Pareto Evolutionary Algorithm. *TIK-report* 103.